Eur. Phys. J. A (2020) 56:143
https://doi.org/10.1140/epja/s10050-020-00153-5

THE EUROPEAN PHYSICAL JOURNAL A

Letter

Mass and half-life measurements of neutron-deficient iodine isotopes

Samuel Ayet San Andrés[1,2,a], Ali Mollaebrahimi[1,3], Timo Dickel[1,2], Julian Bergmann[1], Jens Ebert[1], Hans Geissel[1,2], Florian Greiner[1], Emma Haettner[2], Christine Hornung[1], Nasser Kalantar-Nayestanaki[3], Ivan Miskun[1], Wolfgang R. Plaß[1,2], Sivaji Purushothaman[2], Ann-Kathrin Rink[1], Christoph Scheidenberger[1,2], Helmut Weick[2], Soumya Bagchi[1,2,7], Paul Constantin[6], Andrew Finlay[9], Satbir Kaur[7], Wayne Lippert[1], Israel Mardor[4,5], Bo Mei[6], Iain Moore[8], Jan-Hendrick Otto[1], Stephane Pietri[2], Ilkka Pohjalainen[8], Andrej Prochazka[2], Christophe Rappold[1,2], Moritz P. Reiter[1,9], Yoshiki K. Tanaka[2], John S. Winfield[2], for the Super-FRS Experiment Collaboration

[1] II Physikalisches Institut, Justus-Liebig-Universität Gießen, 35392 Gießen, Germany
[2] GSI Helmholtzzentrum für Schwerionenforschung GmbH, 64291 Darmstadt, Germany
[3] KVI-CART, University of Groningen, Groningen, The Netherlands
[4] Tel Aviv University, 6997801 Tel Aviv, Israel
[5] Soreq Nuclear Research Center, 81800 Yavne, Israel
[6] IFIN-HH/ELI-NP, Măgurele, 077126 Bucharest, Romania
[7] Saint Mary's University, NS B3H 3C3 Halifax, Canada
[8] University of Jyväskylä, 40014 Jyväskylä, Finland
[9] TRIUMF, BC V6T 2A3 Vancouver, Canada

Received: 15 December 2019 / Accepted: 29 April 2020

Communicated by Wolfram Korten

Abstract Neutron-deficient iodine isotopes, ^{116}I and ^{114}I, were produced at relativistic energies by in-flight fragmentation at the Fragment Separator (FRS) at GSI. The FRS Ion Catcher was used to thermalize the ions and to perform highly accurate mass measurements with a Multiple-Reflection Time-of-Flight Mass-Spectrometer (MR-TOF-MS). The masses of both isotopes were measured directly for the first time. The half-life of the ^{114}I was measured by storing the ions in an RF quadrupole for different storage times and counting the remaining nuclei with the MR-TOF-MS. The measured half-life was used to assign the ground state to the measured ^{114}I ions. Predictions on the possible α-decay branch for ^{114}I are presented based on the reduced uncertainties obtained for the Q_α-value. Systematic studies of the mass surface were performed with the newly obtained masses, showing better agreement with the expected trend in this mass region.

1 Introduction

Nuclear masses are basic properties of the nuclei; they reflect the forces between the nucleons. The Q-values, which can be obtained from the masses, define which spontaneous decay modes are energetically possible. In the case of α-decay, the Q-value has a direct correlation to the partial half-life ($T_{1/2}$) of the decaying nuclei, known as the Geiger-Nuttall law [1]. Above the double-magic nucleus ^{100}Sn ($Z = N = 50$) there is a special mid-shell region which forms an island of nuclei with an α-decaying branch. This α-decay island is composed of neutron-deficient isotopes of Te, I, Xe, Cs and Ba [2,3]. Reduced uncertainties in the masses of the nuclides involved in the α-decay can constrain the half-life and, thereby, the expected branching ratio of this decay.

The trend of observables derived from the masses along isotopic or isobaric chains, such as two-proton or two-neutron separation energies (S_{2p}, S_{2n}), can reveal information about nuclear structure [4–6]. These observables can also be used to crosscheck the masses since unexpected changes in the trend of the observables can point towards errors or deviations in the extrapolations of the mass surface. In the α-decaying mid-shell region, the observable calculated from the masses as the double difference of the two-proton separation energy in the Z direction ($d_{2Z}[S_{2p}(N, Z)]$, see Eq. 1), shows some irregularities if the presently known and extrapolated mass values [7] are used.

[a] e-mail: s.ayet@gsi.de (corresponding author)

Published online: 19 May 2020

$$d_{2Z}[S_{2p}(N,Z)] = \frac{S_{2p}(N,Z+2) - 2\cdot S_{2p}(N,Z) + S_{2p}(N,Z-2)}{4} \quad (1)$$

This indicates that inaccuracies may be present in the mass surface in this region. The masses of the iodine isotopes with $N = 61$ (^{114}I) and $N = 63$ (^{116}I) have not been measured directly before, and for the case of ^{114}I only an extrapolated value is available in the literature [7]. Moreover, the decay scheme for the ground and isomeric states of ^{114}I is not well known and has not been published in a primary publication [8].

In this work, we present the first direct mass measurement of ^{116}I and ^{114}I and the half-life measurement of ^{114}I which is used to determine the state of the measured mass distribution. Based on the obtained mass of ^{114}I, an updated value of the Q_α-value with an uncertainty reduced by a factor of 10 is calculated, tightly constraining the α-decay partial half-life of ^{114}I using the Geiger-Nuttall law. Also, a study of the mass surface is presented via the observable $d_{2Z}[S_{2p}(N,Z)]$ showing that the new mass values further refine and smooth the mass surface in this region.

2 Experimental setup and results

2.1 Experimental setup

The nuclides ^{116}I and ^{114}I were produced at relativistic energies via projectile fragmentation at the Fragment Separator (FRS) at GSI [9] and delivered to the FRS Ion Catcher [10] where the ions were slowed down and thermalized in a gas-filled Cryogenic Stopping Cell (CSC) [11–13]. Subsequently, the ions were extracted and transported via a Radio Frequency Quadrupole (RFQ) beamline to a Multiple-Reflection Time-of-Flight Mass Spectrometer (MR-TOF-MS) [14,15] to perform mass measurements and ion counting [16]. The nuclide ^{116}I was produced via fragmentation of a 300 MeV/u ^{238}U projectile beam in a beryllium production target of 0.270 g/cm^2 with intensities up to 2.5×10^8 ions per spill and a typical spill length of 1 s. The CSC was operated at a helium pressure of 64 mbar at a temperature of 77 K, corresponding to an areal density of 4.2 mg/cm^2. For the production of the ^{114}I, a 600 MeV/u projectile beam of ^{124}Xe of up to 1×10^9 ions per spill and a typical spill length of 4 s impinging in a beryllium production target of 1.622 g/cm^2 was used. The CSC was operated at 75 mbar and 82 K, which corresponds to an areal density of 4.6 mg/cm^2. In both cases, an extraction time about 4 times longer than expected was measured due to non-properly working electronics in the RF-Carpet, 200 ms [17,18]. To analyze the data and obtain the masses, the drifts of the time-of-flight data were corrected performing a time-resolved calibration using a well-known mass. The peak shape was obtained from a high-count reference and used for fitting the ion of interest. The analytical function describing the peaks is the Hyper-EMG [19], a weighted maximum likelihood estimate is then used to fit this function to the data. All the measured species reported in this paper are ions singly positively charged. Details of the data analysis procedure are presented in [16].

2.2 Mass of ^{116}I

Previous mass measurements of ^{116}I were performed indirectly [20,21]. The isomeric state of ^{116}I cannot be measured in the MR-TOF-MS due to its short half-life ($t_{1/2}$ = 3.27 μs). The ^{116}I ions underwent 570 isochronous turns (IT) in the analyzer of the MR-TOF-MS. They were then ejected from the analyzer, passed through the Time Focus Shift (TFS) reflector [22] and impinged on the detector. The total time-of-flight amounted to about 19 ms with a resolving power at FWHM of 350.000. The mass range selector (MRS) [15] was used to isolate ions with the mass number $A = 116$ from a total of about 30 species detected in the MR-TOF-MS. A total of 427 counts were recorded for this isotope. The reference ion used for the precision calibration and for the time resolved calibration (TRC) was the molecule ^{86}Kr^{14}N$_2$ (A = 114), which was formed in the CSC and ionized by the beam. It underwent 575 IT in the analyzer of the MR-TOF-MS. This reference ion was included in the spectrum by temporally switching off the MRS. Due to an unfavorable operation of the MRS in this measurement, the MRS shift error [16] is the main source of uncertainty in this mass measurement. Other individual components of the total uncertainty are: peak shape, statistical, calibrant, time-resolved calibration and non-ideal ejection uncertainty (see [16] for more information about the individual contributions).

The mass value for ^{116}I measured in this work, its uncertainty and the deviation from the literature are shown in Table 1. The mass value lies on the upper limit of the uncertainty range reported in the literature for indirect measurements.

2.3 Mass and half-life of ^{114}I

Although the mass of some iodine isotopes with a smaller number of neutrons have already been measured directly [23,24] or indirectly [2,25,26], the mass of ^{114}I has remained unmeasured, and only extrapolated values are available in the literature [7]. The long-lived isomeric state with $t_{1/2} = (6.2\pm0.5)$ s [27] and an excitation energy of 265.9 keV [28] lies almost within the uncertainty range of the extrapolated ground state mass given in the literature, i.e. ± 150 keV [7]. Therefore, if only a single state is detected for this nuclide, the assignment to ground or isomeric state can not be made solely based on its mass.

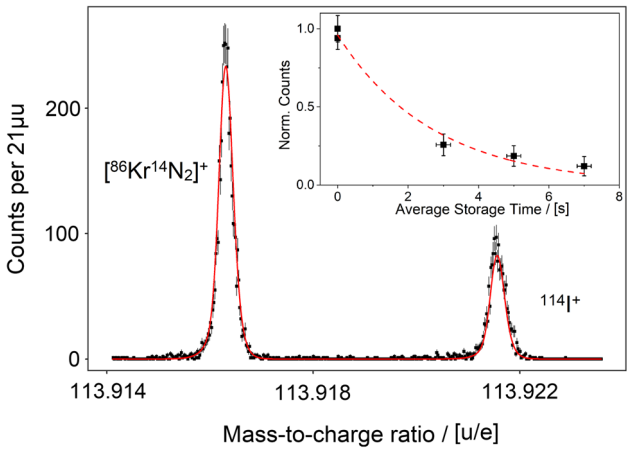

Fig. 1 Measured mass-to-charge ratio spectrum including the calibrant $^{86}Kr^{14}N_2$ (A = 114) and the ion of interest ^{114}I. The square points represent the histogram of the unbinned data. Hyper-EMG functions with one exponential on each side were used for fitting the data, the shape parameters of which were obtained from the calibrant data. The (red) continuous line represent the sum of the two Hyper-EMG functions obtained after fitting the unbinned data. The inset shows the normalized counts of the ^{114}I peak measured for different average storage times in the RFQ. The data points (squares) were normalized to the measurement with the average storage time of 0 s with the highest ^{114}I counts. The (red) dashed curve represents a fit with an exponential decay function, yielding a half-life of (1.89 ± 0.23) s

The mass resolving power at FWHM of the MR-TOF-MS during the measurement with the FRS Ion Catcher was 350.000, enough to distinguish between both states, following the data evaluation method presented in [16]. A detailed investigation of the smallest detectable isomeric ratio was performed by generating and analyzing synthetic data for the given measurement conditions of mass resolving power, distance between the peaks of ground and isomeric state (in this case the excitation energy of the isomer), and the total number of events. The analysis shows that only a single state can be detected if the relative abundance of one of the states is smaller than 10%. For the mass measurement of the nuclide ^{114}I, data with two different numbers of IT were obtained (574 IT and 575 IT) with a total time-of-flight of about 19 ms. The MRS was always on and set to isolate the mass number A = 114. A total of 2775 counts were recorded for the mass measurement of this nuclide. The reference ion for the precision calibration and for the TRC was the same ion as for ^{116}I, namely the isobaric molecule $^{86}Kr^{14}N_2$ (A = 114), which was formed in the CSC and ionized by the beam. The rate of this ion was adjusted by the isolation-dissociation-isolation (IDI) method [29]. A mass-to-charge ratio spectrum including the calibrant ($^{86}Kr^{14}N_2$) and the ion of interest (^{114}I) is shown in Fig. 1. The fitting function determined was a Hyper-EMG with one exponential on each side, the shape parameters of which were calculated from the calibrant data. The result of the data evaluation is represented by the (red) solid line which is the sum of the two Hyper-EMG functions fitted to the unbinned data of the calibrant and ion of interest separately. The areas of the functions were scaled to match the histogram representation, only used to easily visualize the data and results. The individual contributions to the total uncertainty are the same as for ^{114}I but in this case the TRC contribution is the dominant one because the calibrant was not continuously produced. For all mass measurements performed of this nuclide, the data evaluation procedure revealed the presence of a single line in the mass spectrum. This peak was closer to the extrapolated isomer mass (mass excess difference of (-105 ± 151) keV) than to the extrapolated ground state mass (mass excess difference of $+161 \pm 151$ keV). However, if only the mass value is used, both assignments are plausible since the uncertainty of the literature ground state mass is comparable to the excitation energy of the isomer. Therefore, to unambiguously assign the state of the detected single peak another nuclear property has to be measured. In this case, the well-known half-lives of both the ground and the isomeric states, (2.1 ± 0.2) s and (6.2 ± 0.5) s [30], respectively, were used.

The half-life can be measured by counting the surviving nuclei via mass spectrometry after a certain storage time [18,31], and then it can be used to identify the quantum state of the nuclide under consideration [32]. The ^{114}I ions injected in the CSC were extracted and transferred through the RFQ beamline towards the MR-TOF-MS. At the entrance of the MR-TOF-MS, the potential of an aperture was switched to block the ions at the start of the spill injected into the CSC. After a selectable time, the potential was switched back to its normal value. This caused the extracted ions from the CSC to be stored in the RFQ in front of the aperture for an average storage time given by the blocking time of the aperture minus half of the spill length. Note that the ions were always stored for a time longer than the spill length. The average storage times were selected to cover up to at least one half-life of the longer-lived state, namely the isomer with $t_{1/2}$ = 6.2 s and amounted to 0, 3, 5 and 7 s. The spill length was (4 ± 0.2) s. The uncertainty from the spill length takes into account the uniformity and asymmetry of the spill structure and contributes to the uncertainty of the determined half-life. The extraction time from the CSC is negligible in comparison with the average storage time in the RFQ.

The RFQ that was used for the storage of the ions had a inner diameter of 7 mm and was operated with a pseudopotential of about 43 eV and at a pressure of about 0.01 mbar of helium. Therefore, for the ^{114}I ions, the survival efficiency during storage in the RFQ can be assumed to be the same for the different storage times. However, due to their high recoil energy after the β^+ decay, the daughter ions ^{114}Te could not be captured in the RFQ and were lost. The total number of nuclei delivered by the FRS was recorded for each acquisi-

Table 1 Mass and half-life results for the two measured iodine isotopes (^{116}I and ^{114}I) compared with the literature [7,30]. The extrapolated values given in the literature are marked with the symbol #

Nuclei	Half-Life$_{Lit}$/s	Half-Life$_{FRS-IC}$/s	Reference	ME$_{FRS-IC}$/keV	ME$_{AME16}$/keV	ME$_{FRSIC}$-ME$_{AME16}$/keV	Number of events
^{116}I	2.91 ± 0.15	–	^{86}Kr^{14}N$_2$	− 77318 ± 117	− 77490 ± 100	172 ± 154	427
^{114}I	2.1 ± 0.2	1.89 ± 0.23	^{86}Kr^{14}N$_2$	− 72639 ± 20	#− 72800 ± 150	161 ± 151	2775

tion period and used as a normalization factor for the number of ^{114}I nuclei produced. The number of ^{114}I ions after the storage was determined via high-resolution mass measurement using the MR-TOF-MS. An exponential function was fitted to the normalized counts for the different average storage times in order to determine the half-life (see inset in Fig. 1). The uncertainty of the half-life was calculated as the quadratic sum of the statistical uncertainty of the fit (± 0.21 s) and the propagated uncertainty from the spill length (± 0.1 s). The obtained value for the half-life of (1.89 ± 0.23) s is in good agreement with the literature value for the ground state. Thus, the measured mass value could be assigned to the ground state. The results of the mass, half-life and their uncertainties are shown in Table 1.

2.4 Partial half-life of α-decaying iodine isotopes

The island of α-decaying nuclei in the medium-heavy neutron-deficient region comprises iodine ($Z = 53$) isotopes close to the proton drip line, with the lightest reported isotope to have an α-decay branch being ^{108}I [26]. The heaviest iodine isotope with a reported α-decay branch is ^{113}I, with a branching fraction of 3.31×10^{-5}% [2]. For the next iodine isotope (^{114}I), no α-decaying branch has been reported and only estimates have been made from the Q_α-value obtained with masses from the droplet-model [2,33].

The coefficients of the Geiger-Nuttall law [1] for the iodine isotopes were obtained from the existing data on α-decay, from ^{108}I to ^{113}I, obtaining a linear function with a slope of 76.7 and an intercept value of − 39.25. The Q_α-value of ^{114}I, calculated with the literature masses has a large uncertainty, mainly due to the uncertainty of the ^{114}I mass. The $\pm 1\sigma$ uncertainty of the Q_α-value translates in the Geiger-Nuttall law into 3 orders of magnitude of uncertainty in the partial half-life of the ^{114}I α-decay. This is shown in Fig. 2. A more precise determination of the Q_α-value for ^{114}I allows to pin down the partial half-life and, therefore, the branching ratio of the α-decay for this isotope. The α-decay branching ratio for ^{114}I, calculated with the mass values of this work is 7.70×10^{-9}% with a $\pm 1\sigma$ uncertainty below one order of magnitude. This can accurately predict the expected count rate of ^{114}I α-decay and also establish the end of the island of α-emitters in the medium-heavy range of neutron-deficient isotopes, reflected in the low value of the α-decay branching ratio.

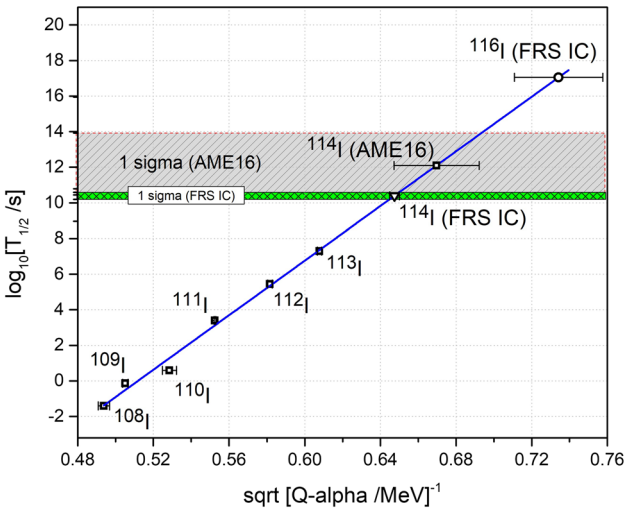

Fig. 2 The logarithm of the partial half-lives vs. Q_α-values for the iodine isotopes. The open squares show the known partial half-lives of the iodine chain reported in AME2016 [7]. These points were used to obtain the constants of the Geiger-Nuttall law [1,34] represented with a (blue) line. The slope of the fitted linear function is 76.7 with an intercept of − 39.25. The hatched gray (left diagonal pattern) area indicates the influence of the $\pm 1\sigma$ Q_α-value uncertainty of the ^{114}I on the partial half-lives. The $\pm 1\sigma$ uncertainty translates into three orders of magnitude change in the α-decay partial half-life (from 10^{10} to $10^{13}s$) for this nucleus. The triangle and circle represent the values calculated from the Geiger-Nuttall law using the the Q_α-values which include the reported ^{114}I and ^{116}I masses presented in this work. The hatched green (vertical line pattern) area indicates the experimentally-reduced Q_α-value uncertainty for partial half-lives with $\pm 1\sigma$ for the ^{114}I. The resulting value in the branching ratio for the ^{114}I α-decay is then significantly constrained to 7.70×10^{-9}% with an $\pm 1\sigma$ uncertainty below one order of magnitude

2.5 Systematic studies of the binding energies

The calculation of the double difference of the two-proton separation energy observable $d_{2Z}[S_{2p}(N, Z)]$ (see Eq. (1)) performed with the masses reported in the literature [7] presents anomalies in the trend in those nuclei where the binding energy of the iodine isotopes (^{114}I and in particular ^{116}I) is included (top panel of Fig. 3). The trend of the $d_{2Z}[S_{2p}(N, Z)]$ values affected by the new mass measurements of the iodine isotopes ($Z = 51$, $Z = 53$, $Z = 55$ and

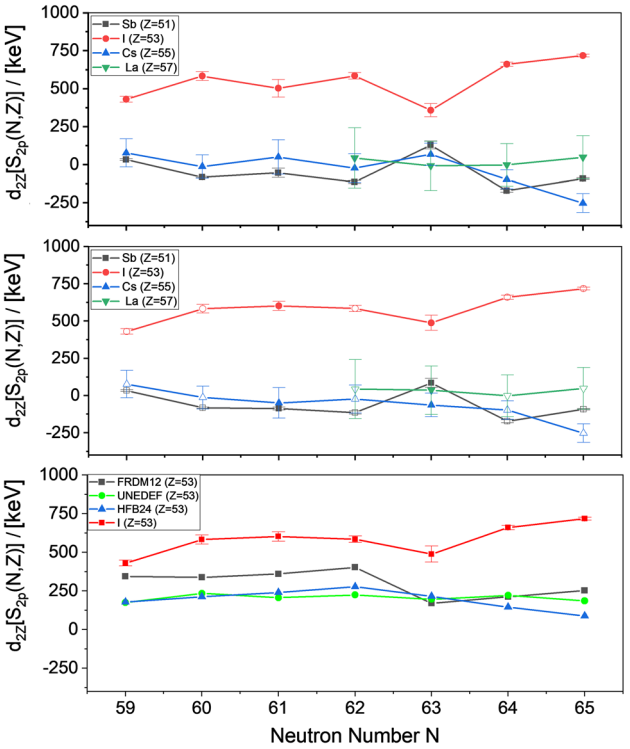

Fig. 3 Double difference of the two proton separation energy in the Z direction $d_{2Z}[S_{2p}(N, Z)]$ (see Eq. (1)) for different isotopic chains calculated with: top: literature mass values [7], middle: literature values including the mass measurement of ^{114}I and ^{116}I presented in this work and bottom: common mass models values (FRDM12 [35], UNEDF1 [36] and HFB-24 [37]) and with the same data as the middle panel for the iodine isotopes for a clear comparison. The filled/empty symbols in the middle panel represent the points which are/are not affected by the new measured masses. The trend of the $d_{2Z}[S_{2p}(N, Z)]$ for the iodine and cesium isotopes is smoother when calculated with the new masses presented in this work (middle panel). The HFB model shows a progressive decrease from N = 62 to N = 65. The FRDM model shows a sudden change at N = 63. The UNEDEF model describes best the general trend of the experimental data and all models agree in the trend if a substantial uncertainty is taken into account

$Z = 57$), shows a smoother behaviour as compared with the literature values of the same nuclei (filled symbols in the middle panel of Fig. 3), in particular for ^{116}I, hinting to a mass discrepancy in the previous indirect mass measurement. A comparison for the $d_{2Z}[S_{2p}(N, Z)]$ values for the iodine chain calculated with different mass models (FRDM12 [35], UNEDF1 [36] and HFB-24 [37]) and the experimental data obtained in this work is shown in the bottom panel of Fig. 3. The HFB model shows a progressive decrease from N = 62 to N = 65 and the FRDM model shows a sudden change at N = 63. The UNEDEF model seem to best describe the general trend of the experimental data. All the models agree in the overall constant trend for the observable if we take into account a substantial uncertainty from the binding energies provided by the mass models. Despite the smoother behaviour of this observable with the new data included, there are still some remaining points where the $d_{2Z}[S_{2p}(N, Z)]$ presents some anomalies in the trend, such as its value for ^{114}Sb. There are also remaining large uncertainties, which prevent accurate identification of the trend, e.g. for the cesium and lanthanum isotopes. The main remaining anomaly seen at ^{114}Sb can be addressed by checking the binding energies of those nuclei included in this observable: ^{114}Sb, ^{112}In (previously measured with a storage ring [38]) and ^{110}Ag (previously measured with indirect methods [39,40]). The large uncertainties of the cesium and lanthanum $d_{2Z}[S_{2p}(N, Z)]$ values are caused by the mass uncertainties of the lanthanum isotopes together with the mass uncertainties of ^{115}Cs and ^{116}Cs, for which only extrapolated mass values are available in the literature [7].

3 Conclusions

First direct mass measurements of ^{116}I and ^{114}I were performed with the MR-TOF-MS at the FRS Ion Catcher (FRS-IC) at GSI. The assignment of the ground and isomeric states for ^{114}I was done based on half-life measurements with the MR-TOF-MS. The new masses measured of ^{114}I and ^{116}I were included in the calculation of the double difference of the two-proton separation energy in the Z direction ($d_{2Z}[S_{2p}(N, Z)]$, see Eq. (1)), showing a better agreement with the expected smooth trend, especially for ^{116}I. This hints to a mass deviation in the previous indirect mass measurement. Using the Geiger-Nuttall law, fitted to the existing α-decaying iodine isotopes, the α-decay branching ratio of ^{114}I was calculated with a significantly reduced uncertainty thanks to the reduction of the Q_α-value uncertainty. A branching ratio of 7.70×10^{-9} with a $\pm 1\sigma$ uncertainty below one order of magnitude was determined, which sets the needs for future experiments in the search of this rare decay mode and which clearly defines the end of the island of α-decaying nuclei for the iodine isotopes.

Acknowledgements Open Access funding provided by Projekt DEAL. This work was supported by the German Federal Ministry for Education and Research (BMBF) under contracts no. 05P12RGFN8, 05P16RGFN1 and 05P19RGFN1, by Justus-Liebig-Universität Gießen and GSI under the JLU-GSI strategic Helmholtz partnership agreement, by HGS-HIRe, and by the Hessian Ministry for Science and Art (HMWK) through the LOEWE Center HICforFAIR.

Data Availability Statement This manuscript has no associated data or the data will not be deposited. [Authors' comment: All data generated during this study are contained in this published article.]

References

1. H. Geiger, J. Nuttall, Lond. Edinb. Dubl. Phil. Mag. **22**, 613 (1911)
2. D. Schardt, T. Batsch, R. Kirchner, O. Klepper, W. Kurcewicz, E. Roeckl, P. Tidemand-Petersson, Nucl. Phys. A **368**, 153 (1981)
3. C. Mazzocchi, Z. Janas, L. Batist, V. Belleguic, J. Döring, M. Gierlik, M. Kapica, R. Kirchner, G. Lalazissis, H. Mahmud et al., Phys. Lett. B **532**, 29 (2002)
4. A. Bohr, B. Mottelson, World Scientific Singapore (1998)
5. E. Leistenschneider, M.P. Reiter, S. Ayet San Andrés, B. Kootte, J.D. Holt, P. Navrátil, C. Babcock, C. Barbieri, B.R. Barquest, J. Bergmann et al., Phys. Rev. Lett. **120**, 062503 (2018)
6. B.S. Ishkhanov, S.V. Sidorov, T.Y. Tretyakova, E.V. Vladimirova, Chin. Phys. C **43**, 014104 (2019)
7. W. Huang, G. Audi, M. Wang, F. Kondev, S. Naimi, X. Xu, Chin. Phys. C **41**, 030002 (2017)
8. J. Blachot, Nucl. Data Sheets **113**, 515 (2012)
9. H. Geissel, P. Armbruster, K. Behr, A. Brünle, K. Burkard, M. Chen, H. Folger, B. Franczak, H. Keller, O. Klepper et al., Nucl. Instrum. Methods B **70**, 286 (1992)
10. W.R. Plaß, T. Dickel, S. Purushothaman, P. Dendooven, H. Geissel, J. Ebert, E. Haettner, C. Jesch, M. Ranjan, M.P. Reiter et al., Nucl. Instrum. Methods B **317**, 457 (2013)
11. M. Ranjan, S. Purushothaman, T. Dickel, H. Geissel, W.R. Plaß, D. Schäfer, C. Scheidenberger, J.V. de Walle, H. Weick, P. Dendooven, Europhys. Lett. **96**, 52001 (2011)
12. S. Purushothaman, M.P. Reiter, E. Haettner, P. Dendooven, T. Dickel, H. Geissel, J. Ebert, C. Jesch, W.R. Plaß, M. Ranjan et al., Europhys. Lett. **104**, 42001 (2013)
13. M. Ranjan, P. Dendooven, S. Purushothaman, T. Dickel, M. Reiter, S. Ayet San Andrés, E. Haettner, I. Moore, N. Kalantar-Nayestanaki, H. Geissel et al., Nucl. Instrum. Methods A **770**, 87 (2015)
14. W.R. Plaß, T. Dickel, U. Czok, H. Geissel, M. Petrick, K. Reinheimer, C. Scheidenberger, M. Yavor, Nucl. Instrum. Methods B **266**, 4560 (2008)
15. T. Dickel, W.R. Plaß, A. Becker, U. Czok, H. Geissel, E. Haettner, C. Jesch, W. Kinsel, M. Petrick, C. Scheidenberger et al., Nucl. Instrum. Methods A **777**, 172 (2015)
16. S. Ayet San Andrés, C. Hornung, J. Ebert, W.R. Plaß, T. Dickel, H. Geissel, C. Scheidenberger, J. Bergmann, F. Greiner, E. Haettner et al., Phys. Rev. C **99**, 064313 (2019)
17. I. Miskun, Ph.D. thesis, Universität Gießen (2019). http://geb.uni-giessen.de
18. I. Miskun, T. Dickel, I. Mardor, C. Hornung, D. Amanbayev, S. Ayet San Andrés, J. Bergmann, J. Ebert, H. Geissel, M. Górska et al., Eur. Phys. J. A **55**, 148 (2019)
19. S. Purushothaman, S. Ayet San Andrés, J. Bergmann, T. Dickel, J. Ebert, H. Geissel, C. Hornung, W.R. Plaß, C. Rappold, C. Scheidenberger et al., Int. J. Mass Spectrom. **421**, 245 (2017)
20. E. Beck, Proceedings International Conference on the Properties of Nuclei Far From the Region of Beta-Stability. **CERN 70-30 1**, pp. 353 (1970)
21. G.M. Gowdy, A.C. Xenoulis, J.L. Wood, K.R. Baker, R.W. Fink, J.L. Weil, B.D. Kern, K.J. Hofstetter, E.H. Spejewski, R.L. Mlekodaj et al., Phys. Rev. C **13**, 1601 (1976)
22. T. Dickel, M.I. Yavor, J. Lang, W.R. Plaß, W. Lippert, H. Geissel, C. Scheidenberger, Int. J. Mass Spectrom. **412**, 1 (2017)
23. V.V. Elomaa, G.K. Vorobjev, A. Kankainen, L. Batist, S. Eliseev, T. Eronen, J. Hakala, A. Jokinen, I.D. Moore, Y.N. Novikov et al., Phys. Rev. Lett. **20019**, 102 (2009)
24. A. Martın, D. Ackermann, G. Audi, K. Blaum, M. Block, A. Chaudhuri, Z. Di, S. Eliseev, R. Ferrer, D. Habs et al., Eur. Phys. J. A **34**, 341 (2007)
25. C. Mazzocchi, R. Grzywacz, S.N. Liddick, K.P. Rykaczewski, H. Schatz, J.C. Batchelder, C.R. Bingham, C.J. Gross, J.H. Hamilton, J.K. Hwang et al., Phys. Rev. Lett. **98**, 212501 (2007)
26. R.D. Page, P.J. Woods, S.J. Bennett, M. Freer, B.R. Fulton, R.A. Cunningham, J. Groves, M.A.C. Hotchkis, A.N. James, Z. Phys. A Hadrons Nuclei. **338**, 295 (1991)
27. B. Zimmermann, Private Communication (1995)
28. A.K. Jain, B. Maheshwari, S. Garg, M. Patial, B. Singh, Nucl. Data Sheets **128**, 1 (2015)
29. F. Greiner, T. Dickel, S. Ayet, J. Bergmann, P. Constantin, J. Ebert, H. Geissel, E. Haettner, C. Hornung, I. Miskun et al., Nucl. Instrum. Methods Phys. Res. B (2019)
30. G. Audi, F.G. Kondev, M. Wang, W.J. Huang, S. Naimi, Chin. Phys. C **41**, 030001 (2017)
31. R. Wolf, D. Atanasov, K. Blaum, S. Kreim, D. Lunney, V. Manea, M. Rosenbusch, L. Schweikhard, A. Welker, F. Wienholtz et al., Nucl. Instrum. Methods Phys. Res. B **376**, 275 (2016)
32. A.T. Gallant, M. Alanssari, J.C. Bale, C. Andreoiu, B.R. Barquest, U. Chowdhury, J. Even, A. Finlay, D. Frekers, G. Gwinner et al., Phys. Rev. C **96**, 024325 (2017)
33. W.D. Myers, Atom. Data Nucl. Data Tables **17**, 411 (1976)
34. C. Qi, A. Andreyev, M. Huyse, R. Liotta, P.V. Duppen, R. Wyss, Phys. Lett. B **734**, 203 (2014)
35. P. Möller, A.J. Sierk, T. Ichikawa, H. Sagawa, Atom. Data Nucl. Data Tables **109**, 1 (2016)
36. M. Kortelainen, T. Lesinski, J. Moré, W. Nazarewicz, J. Sarich, N. Schunck, M. Stoitsov, S. Wild, Phys. Rev. C **82**, 024313 (2010)
37. S. Goriely, N. Chamel, J.M. Pearson, Phys. Rev. C **88**, 024308 (2013)
38. Y. Litvinov, H. Geissel, T. Radon, F. Attallah, G. Audi, K. Beckert, F. Bosch, M. Falch, B. Franzke, M. Hausmann et al., Nucl. Phys. A **756**, 3 (2005)
39. J. Moragues, P. Reyes-Suter, T. Suter, Nucl. Phys. A **99**, 652 (1967)
40. H. Daniel, O. Mehling, D. Schotte, Z. Phys. A **172**, 202 (1963)